JOURNAL OF THE MECHANICAL BEHAVIOR OF BIOMEDICAL MATERIALS 39 (2014) 366–374

Available online at www.sciencedirect.com

ScienceDirect

www.elsevier.com/locate/jmbbm

Research Paper

Determination of the elastic properties of rabbit vocal fold tissue using uniaxial tensile testing and a tailored finite element model

Neda Latifi, Amir K. Miri, Luc Mongeau*

Department of Mechanical Engineering, McGill University, 817 Sherbrooke Street West, Montreal, Canada QC H3A 0C3

ARTICLE INFO

Article history:
Received 27 February 2014
Received in revised form
5 July 2014
Accepted 29 July 2014
Available online 6 August 2014

Keywords:
Biomechanics
Vocal fold
Tensile test
Geometrical models
Inverse problem
Finite element model

ABSTRACT

The aim of the present study was to quantify the effects of the specimen shape on the accuracy of mechanical properties determined from a shape-specific model generation strategy. Digital images of five rabbit vocal folds (VFs) in their initial undeformed conditions were used to build corresponding specific solid models. The displacement field of the VFs under uniaxial tensile test was then measured over the visible portion of the surface using digital image correlation. A three-dimensional finite element model was built, using ABAQUS, for each solid model, while imposing measured boundary conditions. An inverse-problem method was used, assuming a homogeneous isotropic linear elastic constitutive model. Unknown elastic properties were identified iteratively through an error minimization technique between simulated and measured force-time data. The longitudinal elastic moduli of the five rabbit VFs were calculated and compared to values from a simple analytical method and those obtained by approximating the cross-section as elliptical. The use of shape-specific models significantly reduced the standard deviation of the Young's moduli of the tested specimens. However, a non-parametric statistical analysis test, i.e., the Friedman test, yielded no statistically significant differences between the shape-specific method and the elliptic cylindrical finite element model. Considering the required procedures to reconstruct the shape-specific finite element model for each tissue specimen, it might be expedient to use the simpler method when large numbers of tissue specimens are to be compared regarding their Young's moduli.

1. Introduction

The vocal folds, the primary organs of human phonation, are two lips of very soft tissue located on opposite sides of the larynx. Their elastic properties need to fall within a certain range for proper phonation. Accurate engineering methods and data are required to characterize vocal fold tissue. The rabbit animal model has often been used to investigate the vocal fold ultra-structural alterations in clinical problems such as wound healing and scarring (Dahlqvist et al., 2004;

*Correspondence to: Department of Mechanical Engineering, McGill University, 817 Sherbrooke Street West, Montreal, Quebec, Canada H3A 0C3. Tel.: +1 438 938 5383; fax: +1 514 398 7365.
E-mail addresses: neda.latifialavijeh@mail.mcgill.ca (N. Latifi), amir.miriramsheh@mail.mcgill.ca (A.K. Miri), luc.mongeau@mcgill.ca (L. Mongeau).

http://dx.doi.org/10.1016/j.jmbbm.2014.07.031
1751-6161/

Hansen and Thibeault, 2006; Hertegård et al., 2006; Thibeault et al., 2002). The quantification of the rabbit vocal fold mechanical properties, however, presents experimental challenges because the tissue is very soft, and the specimens are very small. Shear rheometry and conventional uniaxial tensile testing have been used in previous studies to quantify the mechanical properties of rabbit vocal folds (Miri et al., 2014; Thibeault et al., 2002). The preparation of standard uniformly shaped test specimens for shear rheometry and conventional uniaxial testing of rabbit vocal folds is impractical because of their tortuous shapes and small dimensions. Thus, there is a need for robust methods that allow testing of specimens with arbitrary shapes.

In uniaxial tensile tests, strain is often estimated as the ratio between the plunger displacement and the gauge length of the specimen in-situ (Alipour and Titze, 1991; Riede et al., 2011). Stress is then estimated as the ratio between the measured force and the average cross-sectional area, assuming a cylindrical specimen shape. But local deformations around the anchor points may significantly bias the estimation of the stretch from the plunger displacement. Local deformation measurements yield more accurate results, as revealed and emphasized in recent studies on human vocal fold tissue. Kelleher et al. (2010) obtained local strain values by means of digital image correlation[1] (DIC). The Young's modulus obtained locally from the ratio of stress and local longitudinal strain was found to be significantly greater than that based on the plunger displacement (Kelleher et al., 2010). Small and soft tissues, such as rabbit vocal folds, often yield results with significant experimental uncertainties (Riede et al., 2011). Errors in the cross-sectional area and the length of the specimen are known to significantly affect the calculated Young's modulus (Cook and Mongeau, 2007).

In an earlier study, finite element analysis has been combined with inverse determination procedures to identify the Young's modulus of porcine vocal fold tissue (Bufi, 2011). The shape of the specimen was approximated as rectangular, which was believed to have caused errors in the results. Shape-specific finite element models have been recently used to estimate the hyper-elastic properties of the human sternocleido-mastoideus muscle from uniaxial tensile testing (Gras et al., 2012). The dependency of vocal fold tissue mechanical properties on the specimen geometrical uncertainties has not yet been systematically investigated. This motivated the present study on the use of uniaxial tensile testing and shape-specific finite element modeling to estimate rabbit vocal fold tissue mechanical properties. The tissue nonlinear, anisotropic, viscoelastic behavior was neglected at this time for the sake of simplicity. A linear isotropic elastic constitutive model was assumed to quantify the influence of tissue specimen shape on its mechanical properties. A shape-specific finite element model[2] (FEM) was created for each one of five rabbit vocal folds, and their elastic moduli were estimated using an inverse determination procedure. The accuracy of the proposed method was first investigated using three synthetic silicon rubber specimens with different shapes and sizes. Then, the method was applied for the actual tissue specimens, and the results were compared with those obtained from approximate methods.

[1]Digital image correlation: DIC.
[2]Finite element model: FEM.

2. Methods

2.1. Specimens

New Zealand rabbits ($n=5$, i.e., two female and three male rabbits) were provided by the animal facility of the department of surgery of the University of Wisconsin in Madison, with the help of Dr. Nicole Li and Professor Susan Thibeault. The larynges were excised and shipped to McGill University at a temperature below $-50\,^{\circ}C$. Following removal of extraneous muscle and shortening of the trachea, as shown in Fig. 1(b), a straight cut was made in the sagittal plane, to create two hemi-larynges (Miri et al., 2014). The right hemi larynx is shown in Fig. 1(c). The vocal folds, which are located between the arytenoid cartilage and the thyroid cartilage, were dissected out of the epiglottis area and the connecting tissues. Portions of the laryngeal wall and of the thyroid cartilage were kept at the anterior and posterior ends of the vocal folds to facilitate gripping the specimen within the testing machine, as shown by the dashed closed curve in Fig. 1(c). The small size of the tissue specimen precluded the removal of the epithelium, which was kept along with the lamina propria and the vocalis muscle.

Synthetic eco-flex 10 Platinum Cure silicon rubber specimens (Smooth-On, Easton, PA) were fabricated using a mixing ratio of 1:1:0.5 (i.e., Eco-flex with one part A, one part B, and 0.5 part silicon thinner) in the laboratory. Following air evacuation, the specimens were molded and cured at room temperature. The synthetic specimens were then trimmed into smooth arbitrary shapes, with no sharp notches or cuts. A typical silicon rubber specimen with arbitrary shape is shown in Fig. 2.

2.2. Experimental procedures

A 3D reconstruction software (iModeller 3D professional, UZR GmbH & Co KG, Hamburg, Germany) was used to construct a three-dimensional solid model of each specimen. This software was selected for its high quality mesh texture based on a previous 3D model reconstruction of the human skull (Abreu et al., 2007). A rotating platform was designed and built for the acquisition of the rabbit tissue specimen images, as shown in Fig. 3(a). The dimensions of the platform enclosure were 10.0 cm × 14.0 cm × 17.0 cm. A fiber-optic light source (Cole-Parmer Instrument Co., Montreal, QC) was used to minimize glare. Three synthetic silicon rubber specimens with different shapes and sizes were prepared, as detailed in Section 2.1. A white speckle pattern was applied on the surface of the synthetic specimens using an enamel spray. The specimens were mounted on the rotating platform in their initial undeformed condition using four black-silk sutures (3.0 metric). A total of 18 planar digital images were captured for each specimen following rotations in equal angular increments of 20°. The superficial layer of the excised rabbit vocal fold tissue is mostly avascular, and thus it was hard to distinguish the boundaries between the tissue and its

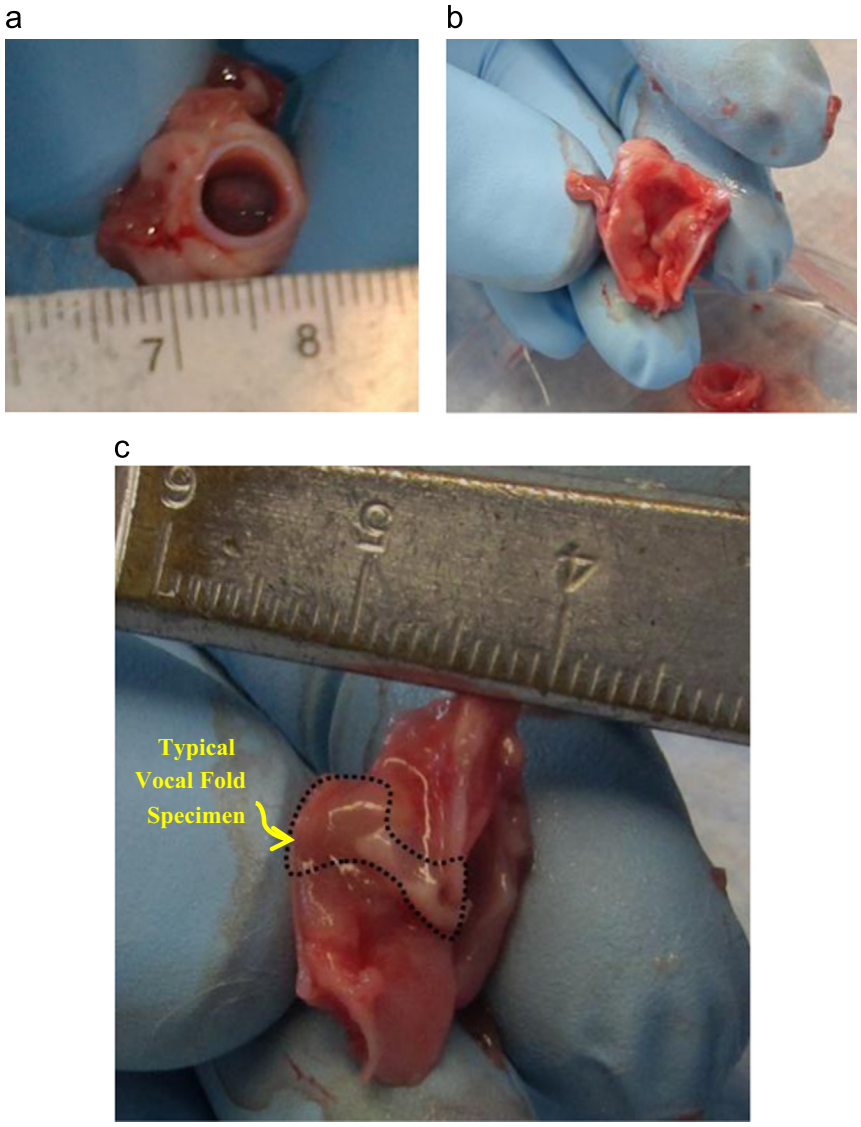

Fig. 1 – Pictures of the rabbit vocal fold dissection procedure. (a) Rabbit larynx observed from the trachea (superior view); (b) the trachea was truncated carefully to reach the location of the two vocal folds; (c) a straight sagittal cut was made to create two hemi larynges. The right hemi larynx is shown. The dashed closed curve shows a typical vocal fold specimen for performing mechanical tensile testing. A ruler was used to provide an estimation of the dimensions of the rabbit vocal fold specimen.

periphery in its natural, pale color. Dark yellow tissue dye was thus used to enhance contrast. Planar digital images were captured for each tissue specimen using the same procedure as for the synthetic silicon rubber specimens (Fig. 3(b)).

An EnduraTEC tester (ElectroForce (ELF) 3200, Bose Inc., Eden Prairie, MN) was used to perform uniaxial traction testing on the tissue and rubber specimens. It was equipped with a digital camera (Flea2, Point Grey Research Inc., Richmond, BC) to record the deformation. The second-axis output signal of the tester was used to trigger the digital camera. The displacement control mode was used, imposing frequency-dependent sinusoidal input waveforms. The sinusoidal displacement was applied at a frequency of 1 Hz with an amplitude varying between 0.5 and 1.5 mm, depending upon the initial undeformed vocal fold length. The vocal folds undergo such deformation when subjected to posturing and adduction–abduction processes (Alipour and Titze, 1991). Non-contact optical measurements were used to measure tissue deformation. A random black speckle pattern was applied onto the tissue using tissue dyes. The presence of the tissue dye was assumed to have negligible effects on the tissue mechanical properties. The specimen was then installed via two-four black-silk sutures in the grips of the tester, as detailed in a previous study (Miri et al., 2012). It was submerged in a normal phosphate buffer solution (PBS) at 37 °C such that a thin layer of fluid covered the epithelium. The fiber-optic light source was used to illuminate the surface of the specimen (Miri et al., 2012).

2.3. Reconstruction of the shape-specific 3D model

Digital planar images of each specimen in its undeformed state were imported and analyzed using iModeller 3D professional. A primary three-dimensional surface model was reconstructed and exported in STL format (Fig. 4(a)). The 3D surface model was imported in SolidWorks 2011 (Dassault Systems SolidWorks Corp., Waltham, MA) using the surface-filling module. The thyroid and arytenoid cartilages were removed from the SolidWorks model. The interface between the vocal fold and the arytenoid and thyroid cartilages was identified based on color. The cartilages were white and the interfaces between the two cartilages and the vocal fold was distinguishable in the recorded images. Fig. 4(b) and (c) shows the model before and after the ablation of the cartilages. The volume of the original and the truncated models was calculated in SolidWorks. The truncated model was then imported in Patran v2010.2 (MSC Software Corporation, Newport Beach, CA) to generate a volume mesh (i.e. four-node tetrahedral elements), as illustrated in Fig. 4(d). The modified model volume was then calculated and compared with that of the truncated model to ensure that the volume mesh was similar to that of the 3D reconstructed surface mesh. The obtained shape-specific FEM was then exported in a text file format, including the nodes, locations, the elements and the connectivity matrix.

Fig. 2 – Picture of an Eco-flex 10 Platinum Cure Silicon Rubber sample with arbitrary shape.

2.4. Finite element analysis

A parametric input file was written using the commercial software ABAQUS 6.10 EF (Dassault Systems Americas Corp., Waltham, MA), assuming a homogeneous isotropic linear elastic constitutive model with two variables, i.e., Poisson's ratio and the longitudinal elastic modulus. A dynamic/explicit finite element analysis was performed. The boundary conditions were imposed to be consistent with the measured experimental conditions, i.e., a zero displacement boundary condition at the interface between the vocal fold lamina propria and the thyroid cartilage, and a sinusoidal longitudinal displacement at the interface between the vocal fold and the arytenoid cartilage. Its amplitude was evaluated based on data obtained from DIC using the correlated software, VIC2D (v2009, Correlated Solutions Inc., Columbia, SC).

A trial and error algorithm was used to obtain the elastic modulus of each tissue specimen. The iterative process started with an initial guess for the elastic modulus as described in Section 2.5. Poisson's ratio was assumed to be 0.495 initially. The time varying reaction forces were calculated using the finite element model and were compared to the measured data. The elastic modulus was modified iteratively until the difference between simulated and measured data was greater than a threshold of 10^{-8}.

In order to validate this method, uniaxial traction testing was performed on three silicon rubber specimens with the

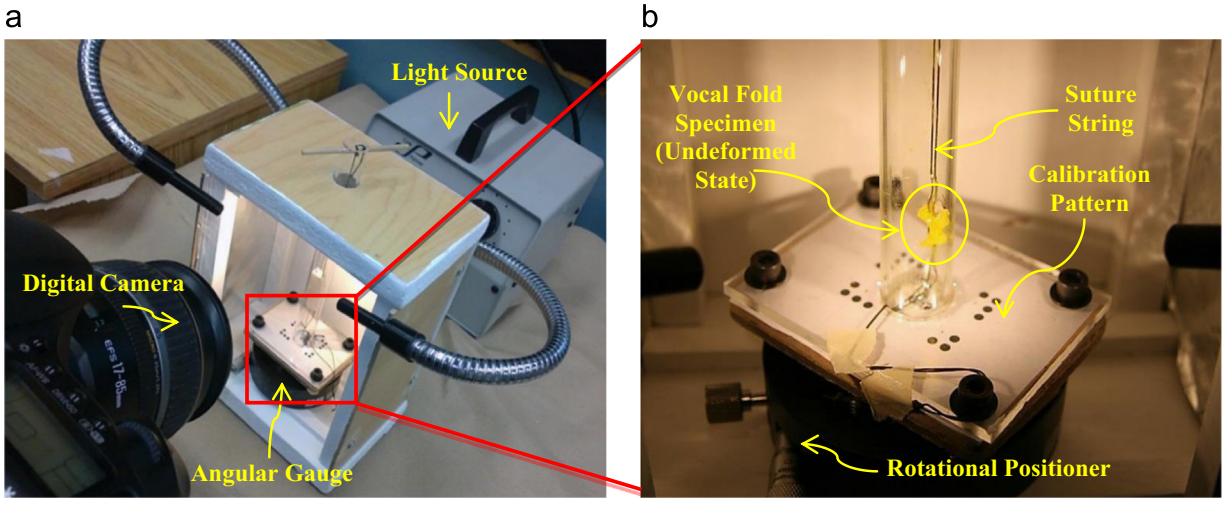

Fig. 3 – Picture of the solid model construction apparatus. (a) The iModeller image acquisition setup; and (b) one of the 2D digital images of an excised rabbit vocal fold specimen in its undeformed state; the vocal fold specimen is originally light pink. It was hard to locate the boundary between the tissue and its environment. To increase the accuracy of the reconstructed 3D model, the tissue was colored in yellow using tissue dye. (For interpretation of the references to color in this figure legend, the reader is referred to the web version of this article.)

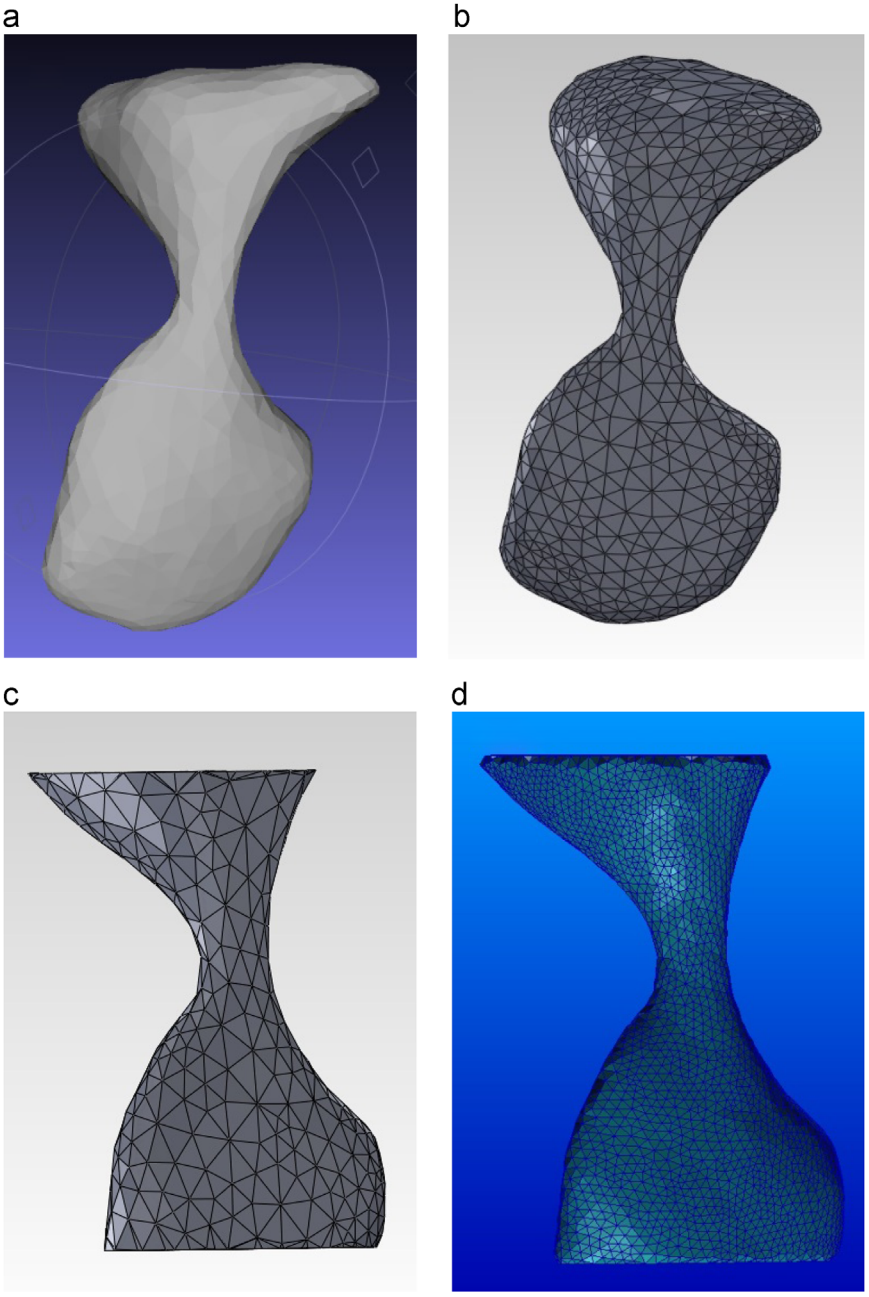

Fig. 4 – Finite Element Model generation; (a) 3D reconstructed surface mesh in iModeller 3D professional; (b) the solid model created in SolidWorks 2011; (c) the solid model after separating the thyroid and arytenoid cartilages; and (d) the final volume mesh generated using MSC Patran 2010.2.

same elastic properties, but different shapes and sizes. For each specimen, three-dimensional solid models and associated FEMs were generated, followed by finite element analysis. The average of the obtained results was compared with that obtained from a previously verified longitudinal wave propagation method (Kazemirad et al., 2013). The finite element analysis was then performed for the five vocal fold specimens using their reconstructed FEMs.

A second set of FEM was created for comparison assuming an elliptic cylindrical geometry with the major axis measured as the average of DIC results. The cross-sectional area was measured at different locations along the longitudinal axis of the shape-specific FEM, and the minor axis was calculated using the average cross-sectional area and the measured major axis. The same finite element analysis procedures were followed for the estimation of elastic modulus, and displacement and strain fields for the simplified model.

2.5. *Theoretical analysis*

The in-plane displacement and strain components were calculated using VIC 2D. The software measures Lagrange strain components on the surface of the tissue. The average longitudinal Lagrange strain component over the central part

of the vocal fold lamina propria was then converted into engineering strain (ε). The nominal stress $\sigma=F/A_o$ was determined based on the average cross-section of the unloaded vocal fold. The longitudinal elastic modulus was obtained using $E=\sigma/\varepsilon$.

3. Results and discussion

3.1. Geometry reconstruction and finite element model generation

Typical example of the reconstructed geometry and the associated finite element model are shown in Fig. 4(a) and (d). Table 1 shows the volume of the tissue specimens, varying between 13.6 mm^3 and 37.7 mm^3. This significant variation may indicate the uncertainty in specimen preparation, associated with the volume fraction of the vocalis muscle. The volume of the truncated solid models and that of the associated FEM was identical within 1.5% for all cases. This supports the accuracy of the procedure to transform the iModeller surface mesh into a volume mesh.

3.2. Validation of the proposed method using synthetic materials

The elastic moduli of three rubber specimens were calculated using the shape-specific method, as summarized in Table 2. The shape-specific method yielded the same elastic modulus for rubber specimens with different shapes and size within the standard deviation of 0.5 kPa. These results were then compared to those from a longitudinal wave propagation method (Kazemirad et al., 2013). The results from the shape-specific finite element analysis and the longitudinal wave propagation method were within 10.0%, as shown in Table 2. The standard deviations of the obtained data were in the same range between the shape-specific (i.e., 0.5 kPa) and wave propagation (i.e. around 0.7 kPa) methods. These results support the accuracy of the shape-specific FEM inverse determination method.

3.3. Shape-specific finite element analysis

Results from the shape-specific FEM are presented in Table 3. Additional results were obtained assuming a cylindrical finite element model with an elliptic cross-section, and the theoretical analysis described in Section 2.5. The assumption of a cylindrical model yielded values about 122.9% different from the shape-specific model results in tissue specimens 1 and 3, and around 26.7% for other three specimens. The simplification of the specimen shape resulted in either an overestimation (i.e., specimens 1, 3, and 4) or an underestimation (i.e., specimens 2 and 5) of the elastic modulus, depending on the dimensions of the vocal fold and the cartilages. By considering the average of the moduli listed in the first column (i.e., 116.8 kPa) and in the second column (i.e., 167.0 kPa) in Table 3, the cylindrical model yields greater values for the tissue Young's modulus compared to the corresponding values obtained using the shape-specific method. Averaging the modulus values for comparing these three methods might cancel out the uncertainties associated with each method as the range of moduli is considerable within specimens. In addition to intrinsic biological differences between various rabbits, such as gender and weight differences, the ratio of the vocalis muscle and the lamina propria was different in the tissue specimens. The average of the absolute relative differences between the results from the two methods was 65.2%. A parametric student's *t*-test was performed using Microsoft Excel 2013, with a significance level of 0.05. The values obtained from the shape-specific finite element model were found to be statistically different from those obtained from the elliptic cylindrical FEM, with a *p*-value of 0.09. Considering the small number of specimens in the present study, a non-parametric K-related statistical analysis test, i.e. the Friedman test, was also performed with a significance level of 0.05, which yielded no statistically significant differences between the shape-specific method and the elliptic cylindrical FEM, with a *p*-value of 1.00. The standard deviation of the five shape-specific tissue moduli was one-half that of the simplified cylindrical FEM (i.e. 53.0 kPa versus 104.3 kPa). The elastic modulus was also calculated analytically, as shown in Table 3. The analytical method yielded values about 50.2% greater than those from the proposed finite element method in specimens 2 and 4. For the three other specimens, the analytical method yielded values about 27.2% smaller than the shape-specific method. The average modulus was around 36.6% greater than that of

Table 2 – Elastic modulus of three Eco-flex silicon rubber specimens obtained from the shape-specific FEM and a wave propagation method.

Specimen ID	Elastic modulus using shape-specific FEM (kPa)	Difference between the current method and longitudinal wave propagation method (%)
Rubber specimen 1	16.2	9.0
Rubber specimen 2	16.2	9.0
Rubber specimen 3	17.0	4.5

Table 1 – Volume of the rabbit vocal fold specimens and their associated finite element models.

Specimen ID	Volume of the truncated reconstructed model (mm^3)	Volume of the finite element model (mm^3)	Difference in volume (%)
Tissue specimen 1	14.2	14.1	0.7
Tissue specimen 2	37.7	37.5	0.5
Tissue specimen 3	20.4	20.3	0.5
Tissue specimen 4	13.6	13.4	1.5
Tissue specimen 5	25.9	25.7	0.8

the shape-specific one. The standard deviation of the analytical results, 85.1 kPa, was also greater than that of the shape-specific results.

The measured displacement and strain fields over the surface were compared to those obtained from the two FEMs (Figs. 5 and 6). The minimum and maximum limits of the color scale were adjusted to be the same in VIC2D and ABAQUS. The shape-specific FEM was found to accurately estimate the longitudinal displacement. The longitudinal strain was also in qualitative agreement with that obtained from DIC. In contrast, the displacement and strain fields from the approximated cylindrical model were significantly different from the DIC results. The similarities between the calculated and measured fields support the accuracy of the shape-specific finite element analysis to estimate the displacement and strain components at different locations. The three-dimensional stress field can also be calculated using the obtained strain field and the calculated Young's modulus.

The average elastic modulus obtained using the current method was observed to be about two orders of magnitude greater than previously published data obtained using parallel-plate rheometers (i.e., 0.5–2 kPa, taking into account the incompressibility assumption) (Cedervall et al., 2007; Hertegard et al., 2009; Thibeault et al., 2002). This may have been caused by the following reasons. The rabbit vocal folds are very small, and the epithelium could not be separated from the lamina propria prior to the tensile testing without losing the mechanical integrity of the tissue. The obtained bulk elastic modulus is thus representative of both the epithelium and the lamina propria, as if the material is homogenous. Furthermore, standard cylindrical specimens could not be prepared from the rabbit vocal folds for the rheological testing. The space between the rheometer plates could not be completely filled up with the tissue from only one vocal fold. Furthermore, a significant difference was previously observed between the tensile test and rheometry

Table 3 – Elastic modulus of rabbit vocal folds obtained using the shape-specific FEM, the elliptic cylindrical FEM, and the analytical approach.

Specimen ID	Shape-specific FEM (kPa)	Elliptic cylindrical FEM (kPa)	Difference between the elliptic cylindrical FEM and the shape-specific FEM (%)	Analytical approach (kPa)	Difference between the analytical approach and the shape-specific FEM (%)
Tissue specimen 1	172.0	300.0	+74.4	106.5	−38.1
Tissue specimen 2	101.0	80.0	−20.8	155.7	+54.1
Tissue specimen 3	70.0	190.0	+171.4	42.7	−39.0
Tissue specimen 4	174.0	220.0	+26.4	256.1	+47.2
Tissue specimen 5	67.0	45.0	−32.8	63.9	−4.6

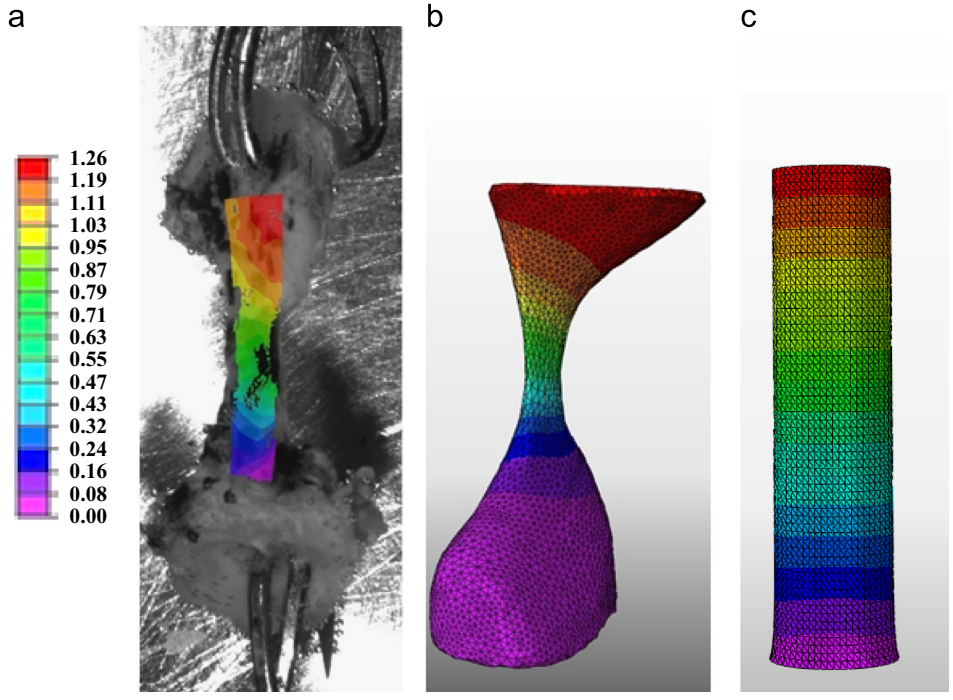

Fig. 5 – (a) Displacement field of the excised rabbit vocal fold tissue using DIC; (b) that of shape-specific FEM; and (c) that of elliptic cylindrical finite element model. The color bar shows the longitudinal displacement of the vocal fold specimen in mm. (For interpretation of the references to color in this figure legend, the reader is referred to the web version of this article.)

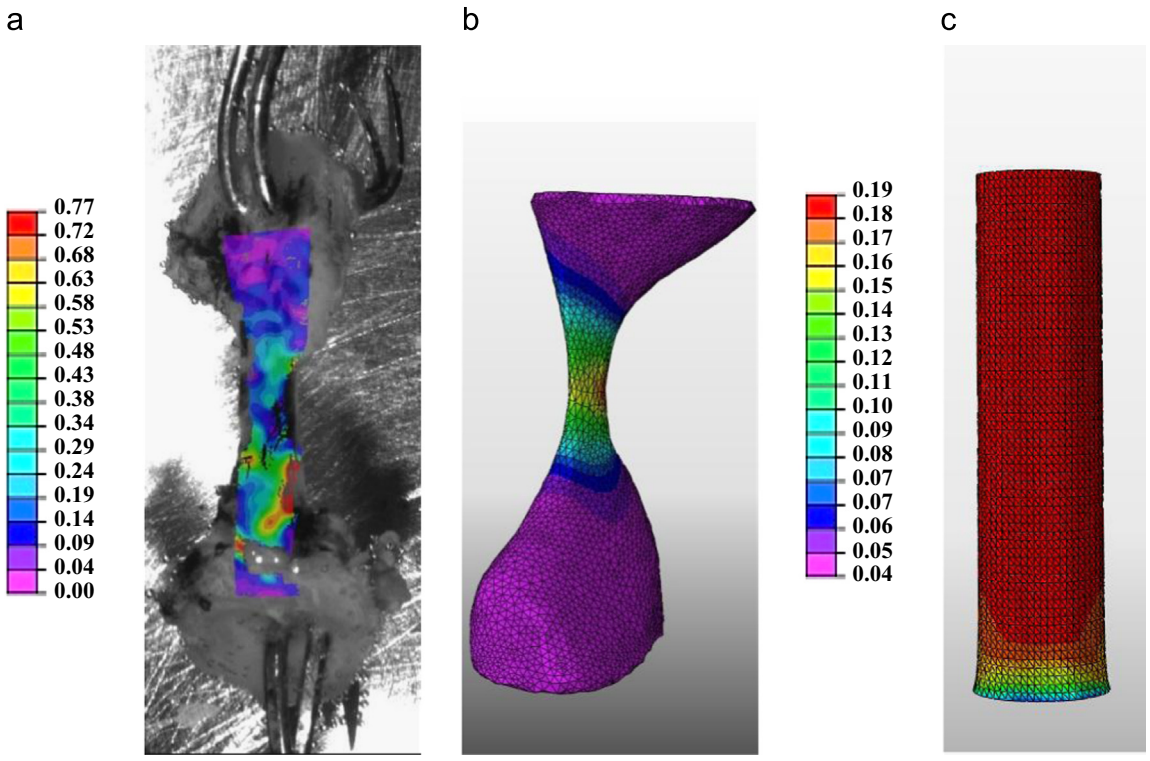

Fig. 6 – (a) The longitudinal strain of the excised rabbit vocal tissue from DIC; (b) that of shape-specific FEM; and (c) that of elliptic cylindrical FEM. The color bar for (a) and (b) is shown in the left. (For interpretation of the references to color in this figure legend, the reader is referred to the web version of this article.)

results for human vocal fold tissue. Kelleher et al. (2010) used a tensile testing method in conjunction with finite element analysis to estimate the elastic modulus of human vocal fold tissue. A circular cross-section geometry was assumed with its outline equal to that of the tissue specimen, and revolved around the longitudinal axis. Large elastic moduli were obtained in comparison with the previously published data obtained using parallel-plate rheometers (Chan and Titze, 1999; Kelleher et al., 2010). The greater values of modulus obtained in the current study may be partly due to the anisotropic properties of the vocal fold tissue (Miri, 2014). It has been previously shown that the longitudinal elastic modulus of vocal fold tissue is at least one order of magnitude greater than the transverse elastic modulus (Heris et al., 2013; Miri et al., 2013). In the present study, the vocal fold tissue intrinsic anisotropy and its time-dependent nonlinear behavior were neglected for the sake of simplicity. It would be preferable to consider anisotropic nonlinear constitutive behavior of the rabbit vocal fold tissue in future studies.

4. Conclusions

The aim of the present paper was to investigate the effects of specimen shape on the mechanical properties of rabbit vocal fold tissue. A homogeneous, isotropic linear elastic constitutive model was used along with a shape-specific FEM. The elastic moduli of five rabbit vocal fold tissues were estimated following an inverse-problem method. The calculated Young's moduli were compared with estimates based on an assumed elliptic cylindrical finite element model, as well as the analytical elastic moduli calculated using a combination of a theoretical tensile test analysis method and digital image correlation. It was found that the use of the shape-specific models yields estimates of Young's modulus within a narrower range of values compared to generic elliptical approximation models. The displacement and strain fields were also found to be qualitatively analogous to the measured data using the shape-specific method. However, a non-parametric statistical analysis showed no statistically significant difference between the two methods. This might be associated with the wide range of values obtained from the generic geometry method. The shape estimation methods suffer from a high perturbation (i.e., uncertainty) in the material properties, and remain unresolved when the moduli of large numbers of specimens are estimated. The proposed shape-specific method is believed to yield a more robust estimate of the bulk elastic modulus of specimens with arbitrary shapes. Further work is needed, however, to confirm this finding for larger number of specimens.

Acknowledgments

This work was supported by Grant NIDCD R01-DC005788 from the National Institutes of Health, (Principal investigator: Luc Mongeau). The authors would like to express their gratitude to Professors Nicole Li and Susan Thibeault (University of Wisconsin, Department of Surgery) for providing the tissue specimens and Professor Rosaire Mongrain (Montreal Heart

Institute, Research Center, Montreal) for sharing his mechanical tester. We are thankful to Juan F. Henao (McGill University, Department of Mechanical Engineering) for his help in preparing the iModeller setup. Finally, the authors would like to express their heartfelt gratitude to the reviewers for their constructive comments.

A partial version of this work was presented in the 8th International Conference on Voice Physiology and Biomechanics, Erlangen, Germany, July 5–7, 2012.

REFERENCES

Abreu, C., Brasil, L., Bernardi, A., Balaniuk, R., Azevedo, F., 2007. 3D Modelling of the human skull. In: Magjarevic, R., Nagel, J.H. (Eds.), World Congress on Medical Physics and Biomedical Engineering 2006, (Vol. 14). Springer, Berlin Heidelberg, pp. 3840–3842.

Alipour, F., Titze, I.R., 1991. Elastic models of vocal fold tissues. J. Acoust. Soc. Am. 90 (3), 1326–1331.

Bufi, N., 2011. Determination of soft tissue material constants using tailored finite element model based regressions (MSc. thesis). McGill University.

Cedervall, J., Ährlund-Richter, L., Svensson, B., Forsgren, K., Maurer, F.H., Vidovska, D., Hertegård, S., 2007. Injection of embryonic stem cells into scarred rabbit vocal folds enhances healing and improves viscoelasticity: short-term results. Laryngoscope 117 (11), 2075–2081.

Chan, R.W., Titze, I.R., 1999. Hyaluronic acid (with fibronectin) as a bioimplant for the vocal fold mucosa. Laryngoscope 109 (7), 1142–1149.

Cook, D.D., Mongeau, L., 2007. Sensitivity of a continuum vocal fold model to geometric parameters, constraints, and boundary conditions. J. Acoust. Soc. Am. 121, 2247–2253.

Dahlqvist, Å., Gärskog, O., Laurent, C., Hertegård, S., Ambrosio, L., Borzacchiello, A., 2004. Viscoelasticity of rabbit vocal folds after injection augmentation. Laryngoscope 114 (1), 138–142.

Gras, L.-L., Mitton, D., Viot, P., Laporte, S., 2012. Hyper-elastic properties of the human sternocleidomastoideus muscle in tension. J. Mech. Behav. Biomed. Mater. 15, 131–140.

Hansen, J.K., Thibeault, S.L., 2006. Current understanding and review of the literature: vocal fold scarring. J. Voice 20 (1), 110–120.

Heris, H.K., Miri, A.K., Tripathy, U., Barthelat, F., Mongeau, L., 2013. Indentation of poroviscoelastic vocal fold tissue using an atomic force microscope. J. Mech. Behav. Biomed. Mater. 28, 383–392.

Hertegård, S., Cedervall, J., Svensson, B., Forsberg, K., Maurer, F.H., Vidovska, D., Olivius, P., Ährlund-Richter, L., Le Blanc, K., 2006. Viscoelastic and histologic properties in scarred rabbit vocal folds after mesenchymal stem cell injection. Laryngoscope 116 (7), 1248–1254.

Hertegard, S., Larsson, H., Nagubothu, S.S.R., Tolf, A., Svensson, B., 2009. Elasticity measurements in scarred rabbit vocal folds using air pulse stimulation. Logop. Phoniatr. Vocol. 34 (4), 190–195.

Kazemirad, S., Heris, H.K., Mongeau, L., 2013. Experimental methods for the characterization of the frequency-dependent viscoelastic properties of soft materials. J. Acoust. Soc. Am. 133, 3186–3197.

Kelleher, J.E., Zhang, K., Siegmund, T., Chan, R.W., 2010. Spatially varying properties of the vocal ligament contribute to its eigenfrequency response. J. Mech. Behav. Biomed. Mater. 3 (8), 600–609.

Miri, A.K., Li, N.Y.K., Avazmohammadi, R., Thibeault, S., Mongrain, R., Mongeau, L., 2014. Study of extracellular matrix in vocal fold biomechanics using a two-phase model. Biomech. Model. Mechanobiol., 1–9, http://dx.doi.org/10.1007/s10237-014-0585-5.

Miri, A.K., 2014. Mechanical characterization of vocal fold tissue: a review study. J Voice, 1–11 http://dx.doi.org/10.1016/j.jvoice.2014.03.001.

Miri, A.K., Heris, H.K., Tripathy, U., Wiseman, P.W., Mongeau, L., 2013. Microstructural characterization of vocal folds toward a strain-energy model of collagen remodeling. Acta Biomater. 9 (8), 7957–7967.

Miri, A.K., Mongrain, R., Chen, L.X., Mongeau, L., 2012. Quantitative assessment of the anisotropy of vocal fold tissue using shear rheometry and traction testing. J. Biomech. 45, 2943–2946.

Riede, T., York, A., Furst, S., Müller, R., Seelecke, S., 2011. Elasticity and stress relaxation of a very small vocal fold. J. Biomech. 44 (10), 1936–1940.

Thibeault, S.L., Gray, S.D., Bless, D.M., Chan, R.W., Ford, C.N., 2002. Histologic and rheologic characterization of vocal fold scarring. J. Voice 16 (1), 96–104.